Research Article | Vol. 31, No. 25 / 4 Dec 2023 / Optics Express 42439
Optics EXPRESS

Tuning the emission properties of electrically pumped semiconductor random lasers via controlled pulsed laser ablation

ANTONIO CONSOLI,[1,2,*] PEDRO DAVID GARCÍA,[1] AND CEFE LÓPEZ[1]

[1] *Instituto de Ciencia de Materiales de Madrid (ICMM), Consejo Superior de Investigaciones Científicas (CSIC), Calle Sor Juana Inés de la Cruz, 3, 28049 Madrid, Spain*
[2] *Escuela de Ingeniería de Fuenlabrada, Universidad Rey Juan Carlos, Camino del Molino 5, 28942, Fuenlabrada, Spain*
[*] *antonio.consoli@urjc.es*

Abstract: Electrically pumped random lasers with distributed feedback can be obtained by introducing random defects into the device active layer, modifying the epitaxial growth process and losing the ease of fabrication potentially offered by disordered structures. We recently demonstrated an alternative and more practical approach in which random lasing emission is obtained from a modified Fabry-Perot laser diode after pulsed laser ablation of its output mirror. Here, we improve our fabrication technique by sweeping the ablating laser beam along the output mirror at different speeds and with different pulse energies, obtaining control over the total energy delivered at each point. We optimize the ablation parameters by evaluating the device performances in terms of lasing threshold and output power and we present the device emission characteristics. The proposed technique is tunable, fast and reliable, allowing the fabrication of devices with different properties by proper selection of the ablation parameters.

© 2023 Optica Publishing Group under the terms of the Optica Open Access Publishing Agreement

1. Introduction

Multiple scattering and optical gain are the fundamental building blocks of random lasers (RLs), providing the optical feedback and amplification required for lasing action [1,2]. With clear applications different from standard lasers, these devices can be used for speckle-free imaging [3], spectroscopy [4], sensing [5] and signal processing [6], due to their multi-mode emission spectrum characterized by narrow randomly distributed frequency peaks or single peaked, strongly coupled modes with low spatial coherence [7]. RLs can be fabricated from different materials, e.g., colloid solutions of dyes and scattering particles [8], polymers [9], crystal powders [10], doped optical fibers [11] or semiconductor where scattering defects are randomly located [12–15]. These approaches are based on a distributed feedback architecture, where gain and multiple scattering are spatially mixed [16,17].

In electrically pumped semiconductor RLs with distributed feedback the introduction of an additional fabrication step during epitaxial growth is required for the introduction of random defects embedded into the active layer. Alternatively, optical gain and scattering elements can be structurally separated in a non-distributed feedback architecture, where the diffusive elements enclose the gain material [18–21]. Following this approach, we previously introduced an electrically pumped RL consisting of the active medium (AlGaInP multi quantum wells, MQWs) enclosed between a mirror and a scattering surface [22]. This device was obtained directly from a commercially available single-transverse mode Fabry-Perot (FP) laser diode (LD) by ablating its output mirror with a high energy femtosecond pulsed laser to obtain a rough and highly scattering surface.

#505673 https://doi.org/10.1364/OE.505673
Journal © 2023 Received 18 Sep 2023; revised 20 Oct 2023; accepted 23 Oct 2023; published 1 Dec 2023

Optics EXPRESS

In our initial approach to fabricate random LDs, we have used a specific and fixed set of parameters in the ablation process. This was sufficient to demonstrate the viability of our approach and focus on the characterization of a single device and its properties. However, our ablation method is intrinsically flexible as the ablating beam properties, e.g., pulse energy, beam diameter, repetition rate, pulse duration or emission wavelength, can be widely varied, providing a sufficiently rich phase space that can be used to control the surface roughness on the output mirror and consequently to tune the spectral and spatial emission characteristics of the modified device.

Here, an ablating pulsed laser beam, with constant beam diameter and pulse energy, is directed onto a LD which is moved so that a pulse train is delivered on the active region section of its output mirror. By varying the speed at which the LD is moved, we can vary the total amount of energy per unit area delivered on the surface, obtaining different surface roughness and disorder. Following this approach, we fabricate several (18) devices with different ablation speeds and variable energy flux on the mirror surface. We present their surface characterization and emission properties in terms of their output power and threshold currents, and we relate the ablation process with the lasing characteristics. We then focus on the behavior of a single device describing its spatial and spectral emission properties. We report that the emission spectra and output patterns vary with current and multi-mode emission is observed that can vary into single mode emission, depending on the injection current.

The fabrication approach proposed here is practical, repeatable, and fast, allowing the realization of a large number of devices in a short time with exotic behavior with multi- and single-mode random lasing emission. The analysis performed relates the effect of the output mirror roughness characteristics on the random LD emission properties and contributes to the experimental characterization of these novel devices. In addition, our work is strongly driven also by application motivations, as the final device performance, e.g. output power and threshold current, can be ameliorated by proper tuning of the ablation parameters.

The manuscript is organized as follows: in Section 2, we present the ablation process and the surface characterization. In Section 3, we describe the emission characteristics of the fabricated random LDs. Finally, in Section 4, we discuss our results and present our conclusions.

2. Fabrication process and surface characterization

The original LDs (Opnext HL6388MG) have an active region composed by AlGaInP MQWs emitting at 637 nm. Modified devices are obtained by ablating the MQW area on the output mirror with a high energy pulsed Nd:YAG laser at 532 nm (Ekspla PL2251C) with linearly polarized light (polarization perpendicular to the plane of the MQWs), 30 ps pulse duration and 10 Hz pulse repetition rate.

To create the roughness on the output mirror, the LD is displaced with a computer-controlled translation stage so that the pulsed laser beam is swept over the entire width of the active area with controllable speed. During the ablation process, the LD is biased with a small amount of current and the active area is imaged in real time on a CCD so that the ablating laser beam is centered on the region of interest.

The pulse energy flux, i.e., the energy per pulse per unit area, F_P, is given by $F_P = E_P\ \pi^{-1}\ (d/2)^{-2}$, being E_P the pulse energy and d the beam diameter. The total energy delivered per unit area of the MQWs cross section is calculated as $F_T = F_P \cdot d \cdot (v \cdot T)^{-1}$, where v is the speed at which the LD is moved and T the pulse period. The total amount of energy delivered to the LD facet is directly proportional to E_P and inversely proportional to v, resulting in higher (lower) amounts of delivered energy when the translation of the LD is slow (fast). Visualization 1 shows the ablation process for $d = 50\,\mu m$, $E_P = 100\,\mu J$ and $v = 60\,\mu m/s$.

We set $d = 50\,\mu m$ and we fabricate two batches of devices: a first batch with $E_P = 100\,\mu J$ and $10\,\mu m/s \le v \le 60\,\mu m/s$, corresponding to $42\ J/cm^2 \le F_T \le 255\ J/cm^2$ and a second batch with

Optics EXPRESS

$E_P = 65$ µJ and 50 µm/s $\leq v \leq 110$ µm/s, corresponding to 15 J/cm^2 $\leq F_T \leq$ 33 J/cm^2 so that we cover the range 15-255 J/cm^{-2}. Ablation parameters are summarized in Table. 1.

Table 1. Ablation parameters of fabricated devices

E_P (µJ)	100						65			
v (µm/s)	10	20	30	40	50	60	50	70	90	110
F_T (J/cm^2)	255	127	85	64	51	42	33	24	18	15
Fabricated devices	1	1	1	1	1	1	3	3	3	3

In selecting the range of v, we consider the following aspects. The highest speed limit, v_{MAX}, is set by the constrain that pulses create a continuous ablated area, a situation in which faster sweep leads to no pulse overlap, i.e., having pulse of diameter d every period T, resulting in $v_{MAX} = d/T = 500$ µm/s. However, we consider that this value results in poor modification of the mirror surface, and we focus our investigation in a significantly lower speed range, with $v = 110$ µm/s being the maximum speed considered. The lowest speed limit is found empirically when no emission is observed due to excessive amount of delivered energy and consequent critical damage of the device. In our experiments, we found this value at $v = 10$ µm/s which corresponds to $F_T = 255$ J/cm^2, for $E_P = 100$ µJ.

In Fig. 1(a) and 1(b), we show the 3D profiles obtained with an optical profilometer (Filmetrics, ProFilm3D) of original and modified devices, respectively.

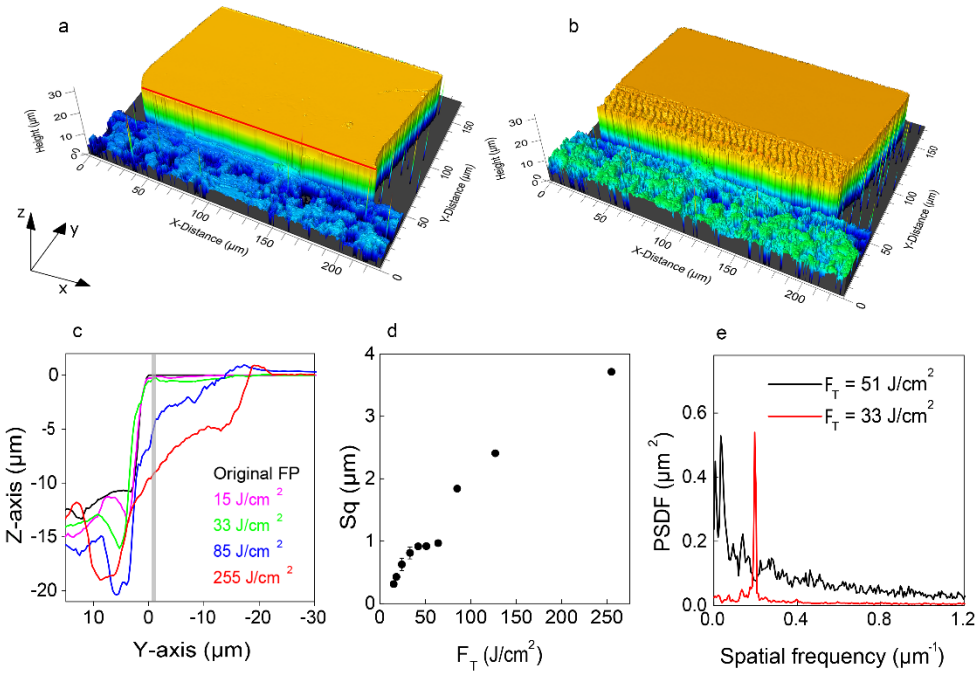

Fig. 1. Optical profilometry of the original (a) and modified (b) device obtained with 33 J/cm^2. Ablation depths obtained with different total energy flux and original LD profile, active region is marked with gray area (c). Calculated root mean square height (Sq) as a function of F_T (d). Power spectral density functions of two devices obtained with $F_T = 33$ J/cm^2 and $F_T = 51$ J/cm^2 (e).

The orange flat surface in Fig. 1(a) is the output mirror of the LD chip, which is located on a silicon substrate (the blue lower rough surface in Fig. 1(a)) for electric and thermal contact.

Optics EXPRESS

The red line in Fig. 1(a) pinpoints the active region, whose center is located at one micrometre from the edge of the chip. The width of the LD chip (x-axis in Fig. 1(a)) is 180 µm and its height (y-axis in Fig. 1(a)) is 100 µm. The output light emission is directed along the z-axis in Fig. 1. The effect of the ablation process is clear in Fig. 1, where the originally flat mirror around the active region (Fig. 1(a)) is transformed into a stripe of rough surface (Fig. 1(b)). The stripe width (along the y-axis direction) is about 25 µm wide, which corresponds to half of the diameter of the ablating beam, as the beam center is located on the active region close to the edge of the chip.

The detail of the z-y profiles obtained with different ablation parameters are plotted in Fig. 1(c): samples ablated at higher F_T present a massive surface removal. In particular, for the highest amount of $F_T = 255$ J/cm^2, the mirror surface is ablated down to the silicon substrate (located at 12 µm below the mirror surface) and for the higher doses some debris can even be seen to accumulate on the outskirts of the ablating spot. For $F_T = 15$ J/cm^2, the ablation depth is below 1 µm, approximately. This trend is observed for all fabricated samples: the ablation depth increases with the delivered energy per unit area.

To quantify the induced roughness of the ablated facets, the root mean square height is calculated, defined in ISO standard 25178 as the standard deviation of the absolute values of heights from the average level of the surface (Sq). Figure 1(d) plots Sq as a function of F_T. Samples fabricated with the lowest amount of delivered energy present the lowest value of the Sq parameter (Sq = 0.9 µm) which increases to Sq = 3.7 µm, as F_T is increased. The average roughness depth is clearly linked to the amount of energy delivered to the LD mirror and decreases with higher target speed or lower pulse energy.

Surface properties of the modified mirrors are also investigated after calculation of their power spectral density function (PSDF), plotted in Fig. 2(e) for two representative samples obtained with $F_T = 33$ J/cm^2 and $F_T = 51$ J/cm^2 both at $v = 50$ um/s. The PSDF is the Fourier transform of the profile autocorrelation function in which any spatial periodicity Δx in the surface is revealed as a peak with a corresponding spatial frequency given by $f_{\Delta x} = 1/\Delta x$. Due to the temporal modulation of the ablation process in which a pulsed laser with a repetition rate T is spatially scanned over the LD surface at speed v, the produced deformation is expected to be periodic with a spatial modulation given by $v \cdot T$. Considering the ablation scanning speed of $v = 50$ µm/s, the corresponding spatial periodicity and frequency are $\Delta x = 5$ µm and $f_{\Delta x} = 0.2$ µm^{-1}, respectively. In Fig. 1(e), a clear peak at $f_{\Delta x} = 0.2$ µm^{-1} is observed only for the lower value of $F_T = 33$ J/cm^2.

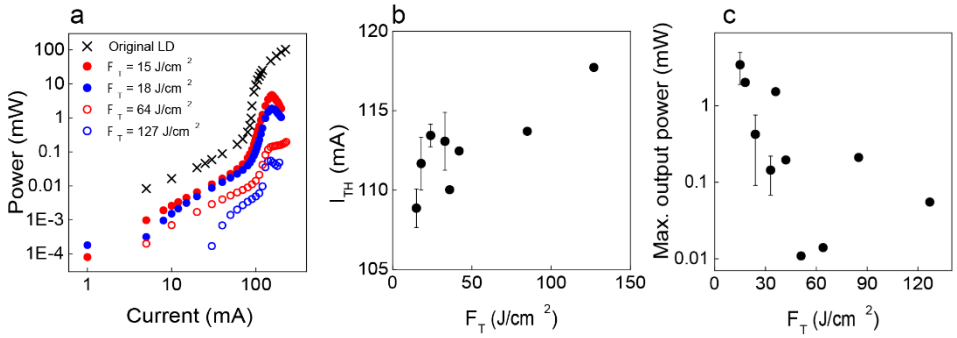

Fig. 2. (a) Output power versus current for different devices: the original FP LD (crosses), and devices obtained with $F_T = 15.1$ J/cm^2 (red dots), $F_T = 18.4$ J/cm^2 (blue dots), $F_T = 64$ J/cm^2 (red circles) and $F_T = 127$ J/cm^2 (blue circles). Threshold current (b) and maximum output power P_{MAX} (c) as a function of F_T, error bars show the standard deviation from measurements performed on three devices.

A similar behavior is observed in other fabricated devices, where the ablation periodicity is detected for low energy fluences, and it is gradually lost at increasing energies. We attribute this

Optics EXPRESS

to a higher degree of randomness in the structure of the ablated surface induced under higher energy levels which smears out any periodicity in the final surface.

3. Emission characteristics

Unmodified devices show typical emission power of 250 mW at 340 mA, threshold current (I_{TH}) around 90 mA and efficiency slope of 0.8 W/A. In original unprocessed devices, emission is observed from the entire width of the active region from the output mirror. Since no current confinement structure is used in these devices and many multiple transverse modes are allowed, the total output power is much higher than in single transverse mode devices.

Devices are biased with CW currents (current driver Thorlabs LDC205C) and temperature stabilized at 20°C (temperature controller Thorlabs TEC200C), unless otherwise specified. The emission from original and modified devices is collected with a microscope objective with a magnification of 50× and a numerical aperture of 0.9 and directed to a calibrated photodiode (Thorlabs, S130C).

Figure 2(a) plots the output power as a function of the bias current for different devices: the original (unprocessed) LD and several random LDs ablated with different amounts of total delivered energy. Lasing devices in Fig. 2(a) clearly show the typical S-curve corresponding to the transition from amplified spontaneous emission to lasing action after crossing the threshold current, to saturation [23,24]. We observe a general trend in the input-output curves: the devices ablated under lower energy fluence present higher values of the maximum output power and lower values of threshold current.

Output power degradation observed in Fig. 2(a) at high bias currents is attributed to heating of the active region in modified devices. We calculated the thermal impedances R_{TH} [25,26] of the original LD and the device ablated with $F_T = 18.4$ μJ/cm^2, obtaining $R_{TH} = 4$°K/W and $R_{TH} = 30$ °K/W, respectively.

We observed amplified spontaneous emission but no lasing action in two fabricated devices obtained with $F_T = 51$ J/cm^2 and with $F_T = 64$ J/cm^2. These two cases of lasing failure are attributed to a possible short-circuit on the ablated mirror caused by localized surface states which provide a less resistive path to injected current. In this case, much less current flows through the optical cavity providing less gain and impeding to reach the lasing regime. We consider that this kind of failure is favored by higher F_T values, for which the modification process is more aggressive.

In Fig. 2(b) we plot the threshold current as a function of F_T, with the error bars corresponding to the standard deviation of the output power from three different devices at each F_T. All the devices present a larger threshold current than the original laser ($I_{TH} = 90$ mA), spanning from $I_{TH} = 108$ mA ($F_T = 15$ J/cm^2) to $I_{TH} = 118$ mA ($F_T = 127$ J/cm^2), as previously observed and attributed to the increase of scattering losses with respect to the original laser [22]. In Fig. 2(c) we plot the maximum output power, P_{MAX}, as a function of F_T. The highest output power is obtained for the lowest ablating energy fluence ($F_T = 15$ J/cm^2) and P_{MAX} decreases as F_T is increased. Two measurements in Fig. 3(c) are found away from the curve trend, resulting in the lowest measured values. These correspond to the non-lasing devices fabricated with $F_T = 51$ J/cm^2 and $F_T = 64$ J/cm^2.

The large standard deviation observed in some samples in Fig. 2(c) is attributed to small differences in the ablation process performed on different devices. In some devices the ablating beam path is not perfectly parallel to the active region, due to a small tilt of the LD when manually placed on the laser mount before the ablation process. This could vary locally the roughness of the ablated mirror if the ablating beam is not perfectly uniform, affecting the output power. Careful alignment of the LD prior to ablation process and a statistical analysis performed on a larger number of devices could clarify this point and possibly reduce the standard deviation of P_{MAX}.

Optics EXPRESS

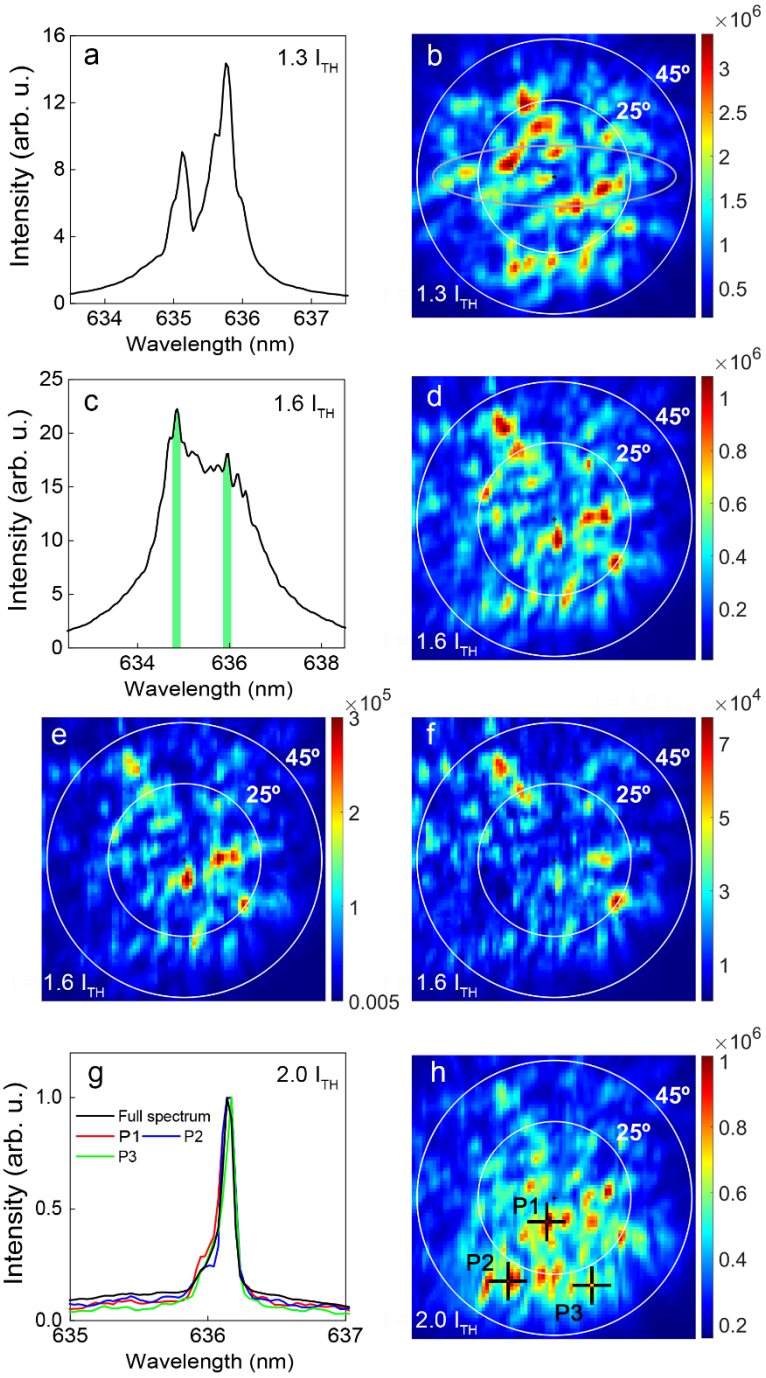

Fig. 3. Emission characterization of the device obtained with $F_T = 42$ J/cm^2, at different bias currents. For $I = 1.3\ I_{TH}$, spectrum (a) and beam profile (b), for comparison the emission profile of the original LD at FWHM is shown with a gray ellipse. For $I = 1.6\ I_{TH}$, spectrum (c), beam profile integrated over the entire wavelength range (d) and over a 0.25 nm wide window at 634.8 nm (e) and 635.96 nm (f). Integration ranges are highlighted with green areas in Fig. 3(c). For $I = 2.0\ I_{TH}$, (g) full spectrum (black line) and spectra collected from three different points P1 (red line), P2 (blue line) and P3 (green line) marked with crosses in the beam profile (h).

Optics EXPRESS

The increase of I_{TH} and decrease of P_{MAX} with F_T are understood as due to the variable degree of damage introduced by the ablation process. High energy fluences results in longer ablation depths, higher Sq and uncorrelated patterns, as shown in Fig. 1, which corresponds to increased losses produced by highly scattering surfaces. The smoother and less aggressive is the ablation process, the better are the emission performances in terms of I_{TH} and P_{MAX}.

The highest value of $P_{MAX} = 4.7$ mW is found when the device is biased with current $I = 1.4 \cdot I_{TH}$, which corresponds to a reduction of the emitted power by a factor of 6 with respect to the original LD when also biased at $I = 1.4\ I_{TH}$. This is a clear improvement with respect to our previous work [22], in which the decrease of output power was of two orders of magnitude after the ablation process (about 40 μW). Previously reported random LDs with distributed feedback [15] show maximum output power of 11 μW and I_{TH} of 25 mA. The higher output obtained in our devices is attributed to the non-distributed feedback architecture in which scattering losses are located on the output rough mirror and do not detriment of the amplification process inside the active region. The obtained I_{TH} cannot be lower than the original I_{TH} (90 mA), as our method introduce additional losses compare to the original FP cavity. Results indicate an increment in I_{TH} of a factor between 1.2 and 1.3 with respect to the original I_{TH}.

In the following we present the spectral and spatial emission characteristics of one device and investigate its operation. The device considered is obtained with $E_P = 100$ μJ and $v = 60$ μm/s corresponding to $F_T = 42$ J/cm^2. Other devices show similar characteristics.

For obtaining spatially resolved spectral measurements, the collimated output beam is scanned with an optical fiber (100 μm core diameter) mounted on computer-controlled translation stages and connected to the spectrometer. A spectrum is collected at each point of the scanned area: the beam pattern is obtained by integrating each collected spectrum over the full wavelength range and the full spectral emission is obtained by summing all the collected spectra. Results obtained for three different currents are shown in Fig. 3.

The full spectral emission and beam pattern obtained for $I = 1.3\ I_{TH}$ are shown in Fig. 3(a) and 3(b), respectively. We observe a double peaked spectrum with peak separation of 0.6 nm and a beam profile with random distribution of maxima and minima of intensity, qualitatively similar to the one observed in our previous work [22]. The emission profile of the original unprocessed LDs is elliptical with full width at half maximum (FWHM) angle of emission of about 15° and 40° in the parallel (x-axis in Fig. 1(a)) and perpendicular (y-axis in Fig. 1(a)) direction of emission, respectively (shown in Fig. 1(b) with gray ellipse).

The spectrum and beam profile obtained for $I = 1.6\ I_{TH}$ are plotted in Fig. 3(c) and 3(d), respectively. At this current the spectrum has a FWHM of 2.1 nm and its profile is characterized by multiple peaks superimposed on a gaussian background. Notably, the emission pattern consists of a speckled profile, as for $I = 1.3\ I_{TH}$, but with a different distribution of maxima and minima of intensity. The spatial emissions of the spectral regions highlighted with green areas in Fig. 3(c) are obtained by numerically integrating the collected spectra in two wavelengths windows (0.25 nm wide) centered at 634.8 nm and 635.96 nm, and shown in Fig. 3(e) and 3(f), respectively. The obtained intensity distributions are different from each other and from the full pattern in Fig. 3(c), as different emission angles correspond to different spectra and the full emission pattern is understood as resulting from the sum of the transverse profiles associated with different frequency peaks.

The spectrum and beam profiles obtained with $I = 2.0\ I_{TH}$ are shown in Fig. 3(g) and 3(h), respectively. In this case the spectrum consists of a single peak with a very narrow FWHM linewidth of 0.12 nm limited by the resolution of the spectrometer. The emission pattern is speckled and different from the beam profiles obtained with other current values, shown in Fig. 3(b) and 3(d). Narrow emission on a single wavelength is observed from all angles of emission. As an example, we show in Fig. 3(g), the normalized full spectrum and three spectra collected from points P1, P2 and P3, highlighted in Fig. 3(h) with black crosses.

Optics EXPRESS

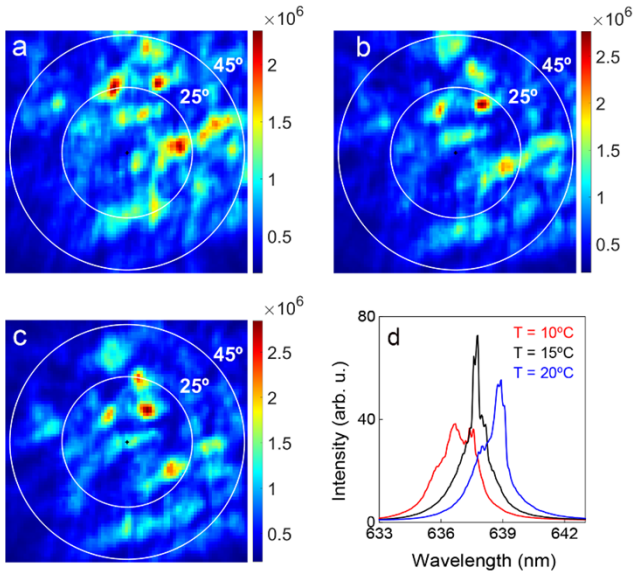

Fig. 4. Output beam profiles obtained from the device fabricated with $F_T = 42$ J/cm^2, when biased with $I = 1.1\ I_{TH}$, at different case temperatures of 10 °C (a), 15 °C (b) and 20 °C (c). (d) Full emission spectra from the same device, with $I = 1.1\ I_{TH}$, at different case temperatures of 10 °C (red line), 15 °C (black line) and 20 °C (blue line).

Devices obtained with different ablation parameters present qualitatively similar emission patterns and spectra compared to the ones shown in Fig. 3. Low values of F_T ($F_T \leq 33$ μJ/cm^2) result in far-fields patterns with larger areas of maximum and minimum intensities and larger spectral widths. The current dependent variation of these properties is observed in all fabricated devices.

The exotic properties observed in Fig. 3 can be summarized as follows: at each current a different spectrum and beam pattern are observed, consisting of single or multiple peaks in frequency and varying speckled directional emission profiles. This behavior is attributed to the variation with current of the longitudinal and transverse modes inside the cavity, which define the spectral and spatial emission of the device. Specifically, the temperature and carrier density variation in the active region due to injected current modifies the refractive index of the cavity, the transverse and longitudinal modes, and their interplay and competition for gain.

Emission on a single wavelength observed for $I = 2.0 \cdot I_{TH}$ is understood as due to strong mode competition between adjacent modes, as theoretically predicted in the framework of coupled mode theory [27,28]. We argue that a strong spatial overlap of longitudinal and transverse modes takes place and only a few modes win the competition for gain, resulting in a very narrow linewidth and one spatial pattern at the output.

In order to verify the hypothesis that the variation of the output beam profile responds to the refractive index change induced by the current-dependent temperature variation, we performed temperature dependent measurements.

In Fig. 4, we show the results obtained with the same device considered in Fig. 3, fabricated with $F_T = 42$ J/cm^2, when biased with a constant current $I = 1.1\ I_{TH}$ and different case temperatures. In Fig. 4(a), 4(b) and 4(c), we show the beam intensity profiles obtained when the case temperature is set to 10 °C, 15 °C and 20 °C, respectively. In Fig. 4(d), the corresponding spectra are plotted. The calculated correlation coefficients between the intensity maps in Fig. 4(a)-(c) range from 0.23 to 0.38, indicating relevant differences in emission patterns at different temperatures. A clear

Optics EXPRESS

change with temperature is also observed in the profile of emitted spectra in Fig. 4(d). These results are attributed to the refractive index change induced by temperature variation.

More in detail, we interpret this behavior with the following picture. In RLs with non-distributed feedback, the longitudinal and transverse lasing modes result from the phase and amplitude contributions of the diffusive mirrors and the cavity path length to the round trip of the resonator [18]. If the refractive index is varied, the optical path changes, thus changing the standing waves, the longitudinal and transverse modes inside the cavity, the emission spectrum and the emission pattern.

4. Discussion and conclusions

In this work we present a method for the fabrication of electrically pumped semiconductor RLs via the modification of the output mirror of commercially available Fabry-Perot LDs. The method relies on the controlled pulsed laser ablation of the output mirror of the original devices, introducing scattering defects which provide the required diffusive feedback for random lasing.

We tested the proposed method with different amounts of total energy delivered, which is varied by varying the speed at which the modified mirror is swept with respect to the ablating beam. Better results, i.e., higher output power and lower threshold current, are obtained from devices ablated with lower amounts of total energy delivered. This is attributed to the degree of disorder induced by our fabrication technique, in which deeper ablation lengths and highly scattering surfaces are obtained for strong ablation energies, resulting in high scattering losses which detrimentally affect the device performances. A complete theoretical model is required for a detailed linking between the scattering properties of the ablated mirror and the emission characteristics of the device. In this work, we limit our contribution to the demonstration of the fabrication method and experimental characterization of the devices.

We demonstrate a maximum output power of 4.7 mW which corresponds to a significant improvement with respect to previous work in which tens of μW were yielded by electrically driven random LDs, demonstrated for the first time.

Critical damage of the original laser and lack of emission after the ablation process have been observed for the one device obtained with the highest amount of ablation energy tested, setting an upper limit to the energy that can be delivered at about 250 J/cm^2. Two devices emit light but do not lase: we suppose that this is due to a low resistance path created by the ablation process on the modified mirror surface which reduce the gain available inside the cavity.

All other devices are fully operational and show clear random lasing emission. We describe in detail the characterization of one device which is qualitatively similar to others. The device considered shows spectral profiles which vary with current and can be characterized by many, few, or a single peak in frequency. The directional emission intensity profile is speckled and varies with current. This behavior is understood as most probably due to the variation of the refractive index of the cavity induced by temperature change provoked by injected current. The multi- or single- peaked spectrum is associated with mode competition and spatial overlapping inside the cavity. This interpretation is supported by the results obtained with temperature dependent measurements which qualitatively reproduce the observed behavior.

We consider that the relevance of the presented work is given by the contributions produced on two sides. On one hand, we demonstrate a flexible, controllable and repeatable technique for simple and fast fabrication of electrically pumped semiconductor RLs with tunable parameters. On the other hand, we report the exotic behavior of one of the manufactured devices with complex dynamics of modal competition resulting in multi- or single- peaked spectra that could find applications in different fields where emission directionality, low coherence, multimode interplay or complex photonic behavior is required.

Funding. Ministerio de Ciencia e Innovación (PDC2022-133418-I00, PID2021-124814NB-C21).

Optics EXPRESS

Acknowledgments. We thank Leo Alvarez and Raul Gago for their help with optical profilometer measurements.

Disclosures. Authors declare no conflicts of interest.

Data availability. Data underlying the results presented in this paper are not publicly available at this time but may be obtained from the authors upon reasonable request.

References

1. D. S. Wiersma, "The physics and applications of random lasers," Nat. Phys. **4**(5), 359–367 (2008).
2. H. Cao, "Random Lasers: Development, Features and Applications," Opt. Photonics News **16**(1), 24–29 (2005).
3. B. Redding, M. a. Choma, and H. Cao, "Speckle-free laser imaging using random laser illumination," Nat. Photonics **6**(6), 355–359 (2012).
4. A. Boschetti, A. Taschin, P. Bartolini, *et al.*, "Spectral super-resolution spectroscopy using a random laser," Nat. Photonics **14**(3), 177–182 (2020).
5. A. N. Azmi, W. Z. Wan Ismail, H. Abu Hassan, *et al.*, "Review of Open Cavity Random Lasers as Laser-Based Sensors," ACS Sens. **7**(4), 914–928 (2022).
6. N. Caselli, A. Consoli, and C. Lopez, "Networks of mutually coupled random lasers," Optica **8**(2), 193 (2021).
7. A. S. L. Gomes, A. L. Moura, C. B. de Araújo, *et al.*, "Recent advances and applications of random lasers and random fiber lasers," Prog. Quantum Electron. **78**, 100343 (2021).
8. L. Yang, G. Feng, J. Yi, *et al.*, "Effective random laser action in Rhodamine 6 G solution with Al nanoparticles," Appl. Opt. **50**(13), 1816 (2011).
9. L. Sznitko, A. Szukalski, K. Cyprych, *et al.*, "Surface roughness induced random lasing in bio-polymeric dye doped film," Chem. Phys. Lett. **576**, 31–34 (2013).
10. J. Azkargorta, I. Iparraguirre, M. Barredo-Zuriarrain, *et al.*, "Random laser action in Nd:YAG crystal powder," Materials (Basel) **9**(5), 369 (2016).
11. S. K. Turitsyn, S. A. Babin, A. E. El-Taher, *et al.*, "Random distributed feedback fibre laser," Nat. Photonics **4**(4), 231–235 (2010).
12. H. K. Liang, B. Meng, G. Liang, *et al.*, "Electrically pumped mid-infrared random lasers," Adv. Mater. **25**(47), 6859–6863 (2013).
13. S. Schönhuber, M. Brandstetter, T. Hisch, *et al.*, "Random lasers for broadband directional emission," Optica **3**(10), 1035 (2016).
14. E. S. P. Leong, S. F. Yu, and S. P. Lau, "Directional edge-emitting UV random laser diodes," Appl. Phys. Lett. **89**(22), 221109 (2006).
15. S. Chu, M. Olmedo, Z. Yang, *et al.*, "Electrically pumped ultraviolet ZnO diode lasers on Si," Appl. Phys. Lett. **93**(18), 181106 (2008).
16. N. M. Lawandy, R. M. Balachandran, A. S. L. Gomes, *et al.*, "Laser action in strongly scattering media," Nature **368**(6470), 436–438 (1994).
17. H. Cao, Y. G. Zhao, H. C. Ong, *et al.*, "Ultraviolet lasing in resonators formed by scattering in semiconductor polycrystalline films," Appl. Phys. Lett. **73**(25), 3656–3658 (1998).
18. A. Consoli and C. López, "Decoupling gain and feedback in coherent random lasers: experiments and simulations," Sci. Rep. **5**(1), 16848 (2015).
19. N. B. Tomazio, L. F. Sciuti, G. F. B. de Almeida, *et al.*, "Solid-state random microlasers fabricated via femtosecond laser writing," Sci. Rep. **8**(1), 13561 (2018).
20. I. B. Dogru-Yuksel, M. Han, G. Pirnat, *et al.*, "High-Q, directional and self-assembled random laser emission using spatially localized feedback via cracks," APL Photonics **5**(10), 106105 (2020).
21. I. B. Dogru-Yuksel, C. Jeong, B. Park, *et al.*, "Silk Nanocrack Origami for Controllable Random Lasers," Adv. Funct. Mater. **31**(45), 2104914 (2021).
22. A. Consoli, N. Caselli, and C. López, "Electrically driven random lasing from a modified Fabry–Pérot laser diode," Nat. Photonics **16**(3), 219–225 (2022).
23. L. A. Coldren, S. W. Corzine, and M. L. Mašanović, *Diode Lasers and Photonic Integrated Circuits* (2012).
24. Anthony E. Siegman, *Lasers* (University Science Books, 1986).
25. W. B. Joyce and R. W. Dixon, "Thermal resistance of heterostructure lasers," J. Appl. Phys. **46**(2), 855–862 (1975).
26. J. S. Manning, "Thermal impedance of diode lasers: Comparison of experimental methods and a theoretical model," J. Appl. Phys. **52**(5), 3179–3184 (1981).
27. A. Consoli and C. Lopez, "Emission regimes of random lasers with spatially localized feedback," Opt. Express **24**(10), 10912–10920 (2016).
28. M. Leonetti, C. Conti, and C. Lopez, "The mode-locking transition of random lasers," Nat. Photonics **5**(10), 615–617 (2011).

48.24.131.129 {ts '2023-12-03 09:02:19'}